Mid-infrared laser operation of Er3+ -doped BaF2 and (Sr,Ba)F2 crystals

Simone Normani, Liza Basyrova, Pavel Loiko, Abdelmjid Benayad, Alain Braud, Ammar Hideur, Patrice Camy

Mid-infrared laser operation of Er^{3+}-doped BaF_2 and $(Sr,Ba)F_2$ crystals

SIMONE NORMANI[1], LIZA BASYROVA[1], PAVEL LOIKO[1], ABDELMJID BENAYAD[1], ALAIN BRAUD[1], AMMAR HIDEUR[2], AND PATRICE CAMY[1,*]

[1]*Centre de Recherche sur les Ions, les Matériaux et la Photonique (CIMAP), UMR 6252 CEA-CNRS-ENSICAEN, Université de Caen, 6 Boulevard Maréchal Juin, 14050 Caen Cedex 4, France*

[2]*CORIA UMR6614, CNRS-INSA-Université de Rouen, Normandie Université, Avenue de l'université, BP. 12, 76801 Saint Etienne du Rouvray, France*

**Corresponding author: patrice.camy@ensicaen.fr*

Received XX Month XXXX; revised XX Month, XXXX; accepted XX Month XXXX; posted XX Month XXXX (Doc. ID XXXXX); published XX Month XXXX

We report on the first mid-infrared laser operation of two Er^{3+}-doped barium-containing fluorite-type crystals, BaF_2 and $(Sr,Ba)F_2$, featuring a low-phonon energy behavior. A continuous-wave 4.9 at.% Er:$(Sr,Ba)F_2$ laser generated 519 mW at 2.79 µm with a slope efficiency of 25.0% and a laser threshold of 27 mW. The vibronic and spectroscopic properties of these crystals are determined. The phonon energy of $(Sr,Ba)F_2$ is as low as 267 cm^{-1}. The Er^{3+} ions in this crystal feature a broadband emission owing to the $^4I_{11/2} \rightarrow {}^4I_{13/2}$ transition and a long luminescence lifetime of the $^4I_{11/2}$ level (10.6 ms) making this compound promising for low-threshold, broadly tunable and pulsed 2.8 µm lasers. © 2022 Optical Society of America

http://dx.doi.org/10.1364/OL.99.099999

Barium fluoride (BaF_2) is a well-known optical material. It is widely used in windows for infrared spectroscopy owing to its broadband transparency (0.15 – 11 µm) and low refractive index (n = 1.469 at 1 µm), as well as a fast scintillator. The growth of undoped crystals by the Bridgman or Czochralski method is well-developed. BaF_2 (called *frankdicksonite* in the mineral form) adopts the cubic fluorite-type structure (sp. gr. $Fm\bar{3}m$) and it can form solid-solutions in the CaF_2 – SrF_2 – BaF_2 system. Unlike its calcium counterpart, BaF_2 has been rarely studied as a host for doping with trivalent rare-earth ions. However, it offers several advantageous properties, namely (i) high thermal conductivity (11.7 $Wm^{-1}K^{-1}$ for undoped crystal) [1] facilitating power-scalable operation, (ii) low phonon energy (242 cm^{-1}) reducing the multiphonon non-radiative path, (iii) higher nonlinear refractive index (as compared to other fluorite-type crystals) and (iv) strong rare-earth ion clustering even at moderate doping levels (>0.5 at.%) [2-4]. The thermal expansion of BaF_2 is relatively high (18.1×10^{-6} K^{-1}) potentially increasing the risk of thermal fracture at high pump levels.

The ion clustering in CaF_2-type crystals leads to a significant inhomogeneous spectral broadening of absorption and emission bands (resembling those for fluoride glasses) [5,6]. This is of particular importance for broadly tunable and mode-locked lasers [7]. Owing to a unique combination of good thermal and spectroscopic properties, Yb^{3+}-doped CaF_2 crystals are currently used in high-energy ultrafast amplifier systems [8]. Recently, Xue *et al.* also reported on a passively mode-locked Yb:BaF_2 laser delivering 52 fs pulses at 1058.2 nm [9].

The ion clustering also promotes energy-transfer processes among the constituent rare-earth ions [10]. Erbium (Er^{3+}) ions are known for their emission in the mid-infrared spectral range, around 2.8 µm [11,12]. 2.8 µm lasers find applications in medicine (laser surgery) due to the strong water absorption of such radiation in soft tissues. The mid-infrared Er^{3+} laser scheme has a self-terminating nature as the lifetime of the lower laser level ($^4I_{13/2}$) is usually longer than that of the emitting state ($^4I_{11/2}$) (the so-called bottleneck effect). Still, CW laser operation is possible due to the energy-transfer upconversion (ETU), $^4I_{13/2} + {}^4I_{13/2} \rightarrow {}^4I_{9/2} + {}^4I_{15/2}$, refilling the upper laser level and emptying the metastable state [13]. For the majority of host matrices, high Er^{3+} doping levels of tens of at.% are needed to reduce the average distance between neighboring ions and to promote ETU [11]. In contrast, for fluorite-type crystals, the dipole-dipole interactions among the Er^{3+} ions forming clusters are greatly enhanced even at low to moderate doping levels [5].

Er^{3+}-doped CaF_2 [14,15] and SrF_2 [16,17] crystals, as well as their solid-solution $(Ca,Sr)F_2$ [18], are known materials for 2.8 µm lasers. Basyrova *et al.* reported on a Ti:Sapphire pumped 4.5 at.% Er:CaF_2 laser delivering 0.83 W at 2800 nm with a high slope efficiency of 31.6% and a laser threshold of 24mW [14]. Further power scaling was recently achieved by Zong *et al.* using diode-pumping: a 1.7 at.% Er:CaF_2 laser generated 2.32 W at 2757 nm at the expense of a lower slope efficiency of 21.2% [15].

Less attention has been paid to their barium counterpart. Considering the lowest phonon energy of BaF_2 (242 cm^{-1}) among all fluorite-type compounds, it is particularly attractive for Er^{3+} doping with the goal of achieving mid-infrared laser emission, due to the expected almost negligible non-radiative path from the $^4I_{11/2}$ state. Recently, Brown *et al.* observed broad mid-infrared emissions from Er^{3+} ions in BaF_2 centered at ~2.75, 3.5, and 4.5 µm [19].

In the present paper, we aimed to study the mid-infrared emission properties of two Er^{3+}-doped barium-containing fluorite-type crystals, namely BaF_2 and $(Sr,Ba)F_2$. The binary solid-solution compositions in the CaF_2 – SrF_2 – BaF_2 system feature lower melting points as compared to their parent compounds, which facilitates the growth of higher optical quality crystals [20,21].

Two fluoride crystals, BaF_2 and $Sr_{0.5}Ba_{0.5}F_2$, doped with 5 at.%

Er^{3+} (nominal concentration) were grown by the Bridgman method using high-purity (4N) BaF_2, SrF_2 and ErF_3 powders in graphite crucibles. The growth chamber was first sealed to vacuum (<10^{-5} mbar) and the growth was performed under Ar + CF_4 atmosphere to prevent the oxygen pollution. The crystal structure (cubic, sp. gr. $Fm\bar{3}m$, fluorite-type) was confirmed by X-ray diffraction. The as-grown crystals had a cylindrical shape (⌀7 mm, length: 30 - 35 mm) and they were transparent and rose colored, as shown in Fig. 1. According to the segregation coefficients for Er^{3+} ions, K_{Er} = ~0.89 and 0.98 for BaF_2 [22] and SrF_2 [16], respectively, the actual doping levels were estimated to be 4.45 at.% (7.48×10^{20} cm^{-3}) and 4.9 at.% (9.09×10^{20} cm^{-3}), respectively.

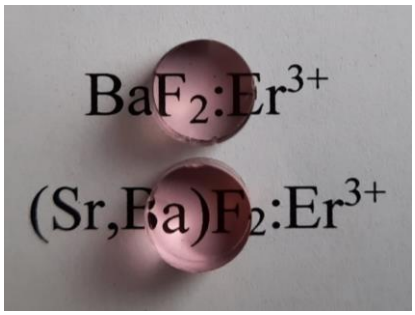

Fig. 1. A photograph of laser-grade polished Er:BaF_2 and Er:(Sr,Ba)F_2 slices cut from as-grown crystal boules.

We studied the vibronic properties of Er^{3+}-doped BaF_2, SrF_2 and (Sr,Ba)F_2 crystals by Raman spectroscopy, see Fig. 2. For all the crystals, only one peak is found in the spectra being characteristic of the cubic fluorite structure (T_{2g} symmetry) [23]. The phonon energy of Er:BaF_2 (242 cm^{-1}) is smaller than that of Er:SrF_2 (285 cm^{-1}) and the Raman peak intensity is higher for Er:BaF_2. For the "mixed" crystal, the Raman peak takes an intermediate position between those for the parent compounds, it is notably broadened and reduced in intensity (FWHM: 25.2 cm^{-1}, compare with 12.4 cm^{-1} for Er:BaF_2), confirming the formation of a substitutional solid-solution with no signatures of different crystalline domains.

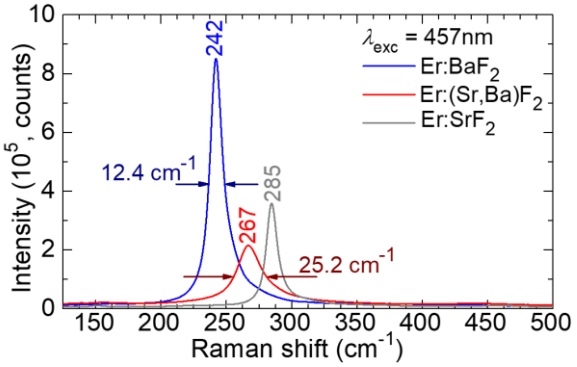

Fig. 2. Raman spectra of Er:BaF_2, Er:SrF_2 and Er:(Sr,Ba)F_2 crystals, λ_{exc} = 457 nm, *numbers* – phonon frequencies.

Prior to laser experiments, the spectroscopic properties of Er^{3+} ions were characterized. Fig. 3(a) shows the Er^{3+} energy-level diagram indicating spectroscopic processes relevant for mid-infrared laser operation. The absorption cross-sections, σ_{abs}, for the $^4I_{15/2} \rightarrow {}^4I_{11/2}$ pump transition are plotted in Fig. 3(b). For Er:(Sr,Ba)F_2, the peak σ_{abs} = 0.30×10^{-20} cm^2 at 971.4 nm and the absorption bandwidth (FWHM) is 9.8 nm. This crystal also exhibits a less structured absorption spectrum as compared to Er:BaF_2. Based on the absorption spectra, the probabilities of spontaneous radiative transitions of Er^{3+} ions were calculated using the standard Judd-Ofelt (J-O) theory. The selected radiative lifetimes τ_{rad} and luminescence branching ratios $\beta_{JJ'}$ are listed in Table 1. For Er:(Sr,Ba)F_2, $\tau_{rad}(^4I_{11/2})$ is 7.55 ms and $\beta_{JJ'}(^4I_{11/2} \rightarrow {}^4I_{13/2})$ = 16.5%.

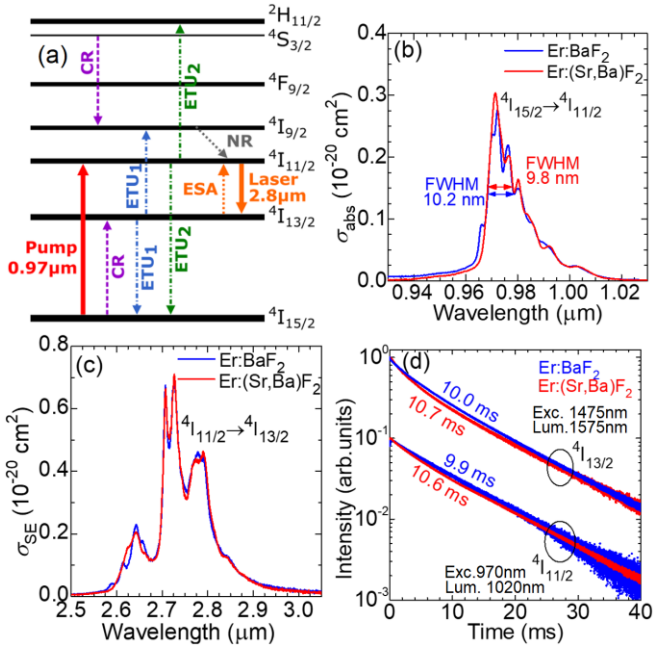

Fig. 3. Spectroscopy of Er^{3+} ions in BaF_2 and (Sr,Ba)F_2 crystals: (a) Er^{3+} energy-level diagram: ETU – energy-transfer upconversion, CR – cross-relaxation, NR – non-radiative decay, ESA – excited-state absorption; (b) absorption cross-sections, σ_{abs}, for the $^4I_{15/2} \rightarrow {}^4I_{11/2}$ transition; (c) SE cross-sections, σ_{SE}, for the $^4I_{11/2} \rightarrow {}^4I_{13/2}$ transition; (d) luminescence decay curves from the $^4I_{11/2}$ and $^4I_{13/2}$ states measured under resonant excitation.

Table 1. Selected Lifetimes[a] and Luminescence Branching Ratios for Erbium Ions in Er:BaF_2 and Er:(Sr,Ba)F_2 Crystals

Crystal	$<\tau_{lum}>$, ms		τ_{rad}, ms		$\beta_{JJ'}$
	$^4I_{13/2}$	$^4I_{11/2}$	$^4I_{13/2}$	$^4I_{11/2}$	$^4I_{11/2} \rightarrow {}^4I_{13/2}$
Er:BaF_2	10.0	9.9	7.52	7.11	16.1%
Er:(Sr,Ba)F_2	10.7	10.6	7.90	7.55	16.5%

[a] τ_{lum} and τ_{rad} – luminescence and radiative lifetime, respectively.

The stimulated-emission (SE) cross-sections, σ_{SE}, for the $^4I_{11/2} \rightarrow {}^4I_{13/2}$ transition falling into the mid-infrared spectral range were calculated using the Füchtbauer–Ladenburg formula [24] using the measured luminescence spectra corrected for the structured water vapor absorption. For Er:(Sr,Ba)F_2, the maximum σ_{SE} is 0.71×10^{-20} cm^2 at 2726 nm and another intense peak appears at longer wavelengths, 2790 nm (σ_{SE} = 0.46×10^{-20} cm^2). Note that for both crystals, the absorption and emission spectra are smooth and broad (a "glassy-like" behavior) which is due to the strong tendency for ion clustering for the studied doping levels. The mean luminescence

lifetimes $<\tau_{lum}>$ of the $^4I_{11/2}$ and $^4I_{13/2}$ Er^{3+} states were measured using finely powdered samples to avoid the effect of radiation trapping and the results are listed in Table 1. For Er:(Sr,Ba)F_2, they are 10.6 ms and 10.7 ms, respectively, representing a favorable ratio for the mid-infrared laser operation. Note that both lifetimes are still longer that the radiative ones, which is ascribed to inevitable dipole-dipole interaction in Er^{3+} clusters. The closeness of the radiative and luminescence lifetimes of the $^4I_{11/2}$ state indicates a very weak non-radiative path from this level which is a consequence of the low-phonon-energy behavior of barium-containing crystals.

The scheme of the mid-infrared laser is shown in Fig. 4(a). The cylindrical laser elements were cut from the central part of the as-grown boules (⌀7 mm, thickness: 6.7 and 7.0 mm for BaF_2 and (Sr,Ba)F_2 respectively). They were polished to laser-grade quality on both sides and left uncoated. The elements were mounted on a passively-cooled Cu-holder using a silver paint for better heat dissipation. We have used a hemispherical laser cavity formed by a flat pump mirror (PM) coated for high transmission (HT, T = 85.7%) at 0.97 μm and for high reflection (HR) at 2.6 – 3.0 μm, and a set of concave (radius of curvature, RoC = -100 mm) output couplers (OC) having a transmission T_{OC} of 0.33% - 4% at 2.7 – 2.9 μm. The crystal was placed close to the PM with an air gap of less than 1 mm, and the geometrical cavity length was ~99 mm. The pump source was a CW Ti:Sapphire laser delivering up to 3.2 W at 971.4 nm (the $^4I_{15/2} \rightarrow {}^4I_{11/2}$ Er^{3+} absorption peak) with almost diffraction-limited beam quality ($M^2 \approx 1$). It output was focused into the laser crystal through the PM using an antireflection-coated achromatic lens (focal length: f = 75 mm) resulting in a pump spot size of $2w_P$ = 125 ± 5 μm. The pumping was in single-pass. The measured pump absorption was 83.8% for Er:BaF_2 and 82.8% for Er:(Sr,Ba)F_2. The pump beam was optionally modulated using a mechanical chopper (duty cycle: 1:3). The residual pump after the OC was filtered out using a long-pass filter (Spectrogon, LP1400). The laser spectra were recorded using a using a ZrF_4 fiber (Thorlabs) and a spectrum analyzer (Bristol, 771 series). The laser mode profile in the far-field was captured using a camera (Pyrocam IIIHR, Ophir-Spiricon) and the M^2 parameter was evaluated using an ISO-standard procedure and the optical knife method for measuring the beam diameters.

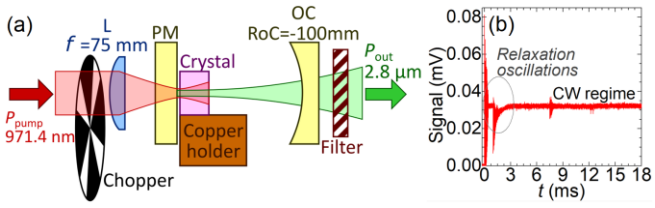

Fig. 4. (a) Scheme of the laser setup: L – achromatic lens, PM – pump mirror, OC – output coupler; (b) a typical oscilloscope trace of the mid-infrared laser emission from Er:(Sr,Ba)F_2.

The power transfer characteristics for Er:BaF_2 and Er:(Sr,Ba)F_2 crystals are shown in Fig. 5(a,b). The Er:BaF_2 laser generated a maximum output power of 350 mW at 2792 nm with a slope efficiency η of 17.2% (vs. the absorbed pump power) and a laser threshold P_{th} of 26 mW (for T_{OC} = 1.7%). With decreasing output coupling from 4% to 0.33%, P_{th} gradually decreased from 93 mW to 17 mW. Such a low-threshold behavior is assigned to the long luminescence lifetime of the upper laser level ($^4I_{11/2}$). The mid-infrared laser performance was improved when using the "mixed" crystal mainly owing to its better optical quality: the Er:(Sr,Ba)F_2 laser was scaled up to 519 mW at 2792 and 2794 nm with a higher slope efficiency of 25.0% and a similar laser threshold of 27 mW (for T_{OC} = 1.7%). The laser emission was unpolarized. By implementing the chopper, no noticeable improvement of the laser performance was achieved. The observed CW mid-infrared operation of Er:BaF_2 and Er:(Sr,Ba)F_2 crystals doped just with 5 at.% Er^{3+} is due to the greatly enhanced ETU in ion clusters which helps to overcome the self-terminating nature of the $^4I_{11/2} \rightarrow {}^4I_{13/2}$ transition.

The round-trip passive loss L was estimated using a model of a quasi-four-level laser accounting for the reabsorption at the laser wavelength [25] (originating from ESA, $^4I_{13/2} \rightarrow {}^4I_{11/2}$) yielding L = 1.7% for Er:BaF_2 and 0.7% for Er:(Sr,Ba)F_2. For the latter crystal, this corresponds to an absorption coefficient of 0.006 cm^{-1}.

The typical spectra of laser emission measured well above the laser threshold are shown in Fig. 5(c,d). They are weakly dependent on the output coupling.

An oscilloscope trace of the mid-infrared laser emission from the Er:(Sr,Ba)F_2 crystal is shown in Fig. 4(b). It reveals relaxation oscillations after switching on the pump followed by CW operation.

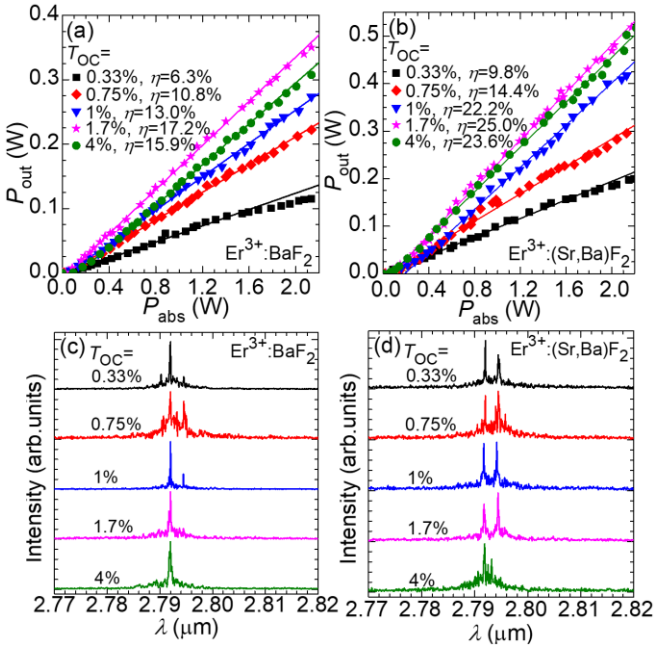

Fig. 5. Mid-infrared (a,c) Er:BaF_2 and (b,d) Er:(Sr,Ba)F_2 lasers: (a,b) input-output dependences, η - slope efficiency, (c,d) spectra of laser emission measured well above the laser threshold.

The spectra of laser emission for both studied crystals were pump-dependent near the laser threshold. Figure 6 illustrates this behavior for the case of Er:(Sr,Ba)F_2. At very low absorbed pump powers (<70 mW), the laser emitted at 2729 nm corresponding to the main emission peak of the $^4I_{11/2} \rightarrow {}^4I_{13/2}$ transition. Then, other laser lines at 2792 nm and 2794 nm appeared, and the latter one became dominant with increasing absorbed pump power. Due to the existence of a resonant ESA channel $^4I_{13/2} \rightarrow {}^4I_{11/2}$ (reabsorption) and a long luminescence lifetime of the terminal laser level, the laser tends to operate according to the quasi-three-level laser scheme, so that the laser spectra vary with the inversion ratio which is pump-dependent. The observed laser lines are also determined by the

structured water vapor absorption in air.

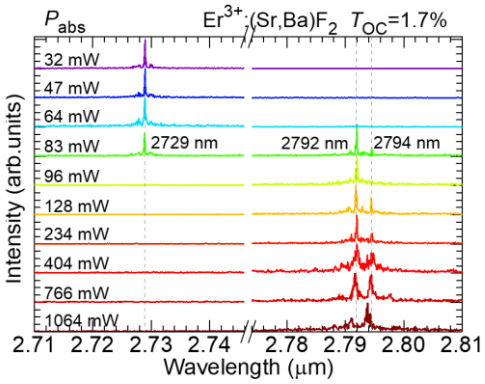

Fig. 6. Dependence of the laser emission spectra of Er:(Sr,Ba)F_2 on the absorbed pump power, T_{OC} = 1.7%.

The far-field beam profile of the Er:(Sr,Ba)F_2 laser is shown in Fig. 7(a). It is only slightly asymmetric and the 1D intensity profiles are well fitted with a Gaussian function. The evaluation of the beam propagation factor is shown in Fig. 7(b). At the maximum pump power, the measured M^2 = 1.08 confirming the laser operation at the fundamental transverse mode.

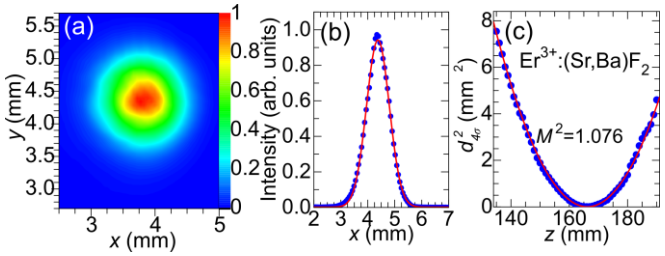

Fig. 7. Spatial characteristics of mid-infrared laser emission from Er:(Sr,Ba)F_2: (a) a typical beam profile in the far-field; (b) a 1D intensity profile showing a Gaussian fit; (c) evaluation of the M^2 parameter, T_{OC} = 1.7%, P_{abs} = 2.2 W.

To conclude, we report on the first mid-infrared laser operation of Er:BaF_2 and Er:(Sr,Ba)F_2 crystals, to the best of our knowledge. These materials benefit from (i) very low phonon energies, (ii) long luminescence lifetime of the upper laser level and a favorable $^4I_{11/2}/^4I_{13/2}$ lifetime ratio, (iii) smooth and broad emission spectra around 2.8 μm owing to the ion clustering, (iv) good thermal properties of the host matrix (for BaF_2) and (v) reduced growth temperature (for the "mixed" compound), making them attractive for the development of power-scalable and broadly tunable mid-infrared lasers. Further power scaling is expected using diode-pumping. An optimization of the Er^{3+} doping level seems to be a key point for increasing the laser efficiency by balancing the crystal quality, its thermal properties, pump absorption and ETU efficiency. Due to the very low phonon energy of Er:BaF_2 approaching that for chloride crystals (203 cm^{-1} for KPb_2Cl_5), this compound may be potentially considered for ~3.5 μm lasers (the $^4F_{9/2} \rightarrow {}^4I_{9/2}$).

Funding. Agence Nationale de la Recherche (ANR-19-CE08-0028); Région Normandie (Chaire d'excellence "RELANCE").

Disclosures. The authors declare no conflicts of interest.

Data availability. Data underlying the results presented in this paper are not publicly available at this time but may be obtained from the authors upon reasonable request.

References

1. D. T. Morelli and J. Heremans, J. Appl. Phys. **63**, 573 (1988).
2. V. Petit, P. Camy, J. L. Doualan, X. Portier, and R. Moncorgé, Phys. Rev. B **78**, 085131 (2008).
3. S. Renard, P. Camy, A. Braud, J. L. Doualan, and R. Moncorgé, J. Alloys Compd. **451**, 71 (2008).
4. B. Lacroix, C. Genevois, J. L. Doualan, G. Brasse, A. Braud, P. Ruterana, P. Camy, E. Talbot, R. Moncorgé, and J. Margerie, Phys. Rev. B **90**, 125124 (2014).
5. C. Labbe, J.L. Doualan, P. Camy, R. Moncorgé, and M. Thuau, Opt. Commun. **209**, 193 (2002).
6. F. Druon, S. Ricaud, D. N. Papadopoulos, A. Pellegrina, P. Camy, J. L. Doualan, R. Moncorgé, A. Courjaud, E. Mottay, and P. Georges, Opt. Mater. Express **1**, 489 (2011).
7. G. Machinet, P. Sevillano, F. Guichard, R. Dubrasquet, P. Camy, J.L. Doualan, R. Moncorgé, P. Georges, F. Druon, D. Descamps, and E. Cormier, Opt. Lett. **38**, 4008 (2013).
8. E. Kaksis, G. Almási, J.A. Fülöp, A. Pugžlys, A. Baltuška, and G. Andriukaitis, Opt. Express, **24**, 28915 (2016).
9. W.-Z. Xue, Z.-L. Lin, H.-J. Zeng, G. Zhang, P. Loiko, L. Basyrova, A. Benayad, P. Camy, V. Petrov, X. Mateos, L. Wang, and W. Chen, Opt. Express **30**, 15807 (2022).
10. P. Loiko, A. Braud, L. Guillemot, J. L. Doualan, A. Benayad, and P. Camy, Proc. SPIE **11357**, 113570N (2020).
11. T. Jensen, A. Diening, G. Huber, and B. H. T. Chai, Opt. Lett. **21**, 585 (1996).
12. M. Bernier, D. Faucher, N. Caron, and R. Vallée, Optics Express **17**, 16941 (2009).
13. M. Pollnau, W. Lüthy, H. P. Weber, T. Jensen, G. Huber, A. Cassanho, H. P. Jenssen, and R. A. McFarlane, Opt. Lett. **21**, 48 (1996).
14. L. Basyrova, P. Loiko, J.-L. Doualan, A. Benayad, A. Braud, B. Viana, and P. Camy, Opt. Express **30**, 8092 (2022).
15. M. Zong, Y. Wang, Z. Zhang, J. Liu, L. Zhao, J. Liu, and L. Su, J. Lumin. **250**, 119089 (2022).
16. W. Ma, X. Qian, J. Wang, J. Liu, X. Fan, J. Liu, L. Su, and J. Xu, Sci. Rep. **6**, 36635 (2016).
17. R. Švejkar, J. Šulc, H. Jelínková, V. Kubeček, W. Ma, D. Jiang, Q. Wu, and L. Su, Opt. Mater. Express **8**, 1025 (2018).
18. J. Liu, X. Feng, X. Fan, Z. Zhang, B. Zhang, J. Liu, and L. Su, Opt. Lett. **43**, 2418 (2018).
19. E. E. Brown, Z. D. Fleischman, J. McKay, and M. Dubinskii, Opt. Mater. Express **11**, 575 (2021).
20. D. Klimm, M. Rabe, R. Bertram, R. Uecker, and L. Parthier, J. Cryst. Growth, **310**, 152 (2008).
21. R.H. Nafziger, J. Am. Ceram. Soc. **54**, 467 (1971).
22. I. Nicoara, M. Stef, G. Buse, and A. Racu, J. Cryst. Growth **547**, 125817 (2020).
23. R. Gee, D.C. O'Shea, and H.Z. Cummins, Solid State Commun. **4**, 43 (1966).
24. F. Aull and H. P. Jenssen, IEEE J. Quantum Electron. **18**, 925 (1982).
25. J. M. Serres, V. Jambunathan, P. Loiko, X. Mateos, H. Yu, H. Zhang, J. Liu, A. Lucianetti, T. Mocek, K. Yumashev, and U. Griebner, Opt. Mater. Express, **6**, 46 (2016).

Full references

1. D. T. Morelli and J. Heremans, "Thermal conductivity of single - crystal barium fluoride," J. Appl. Phys. **63**(2), 573-574 (1988).
2. V. Petit, P. Camy, J. L. Doualan, X. Portier, and R. Moncorgé, "Spectroscopy of Yb^{3+}:CaF_2: From isolated centers to clusters," Phys. Rev. B **78**(8), 085131 (2008).
3. S. Renard, P. Camy, A. Braud, J. L. Doualan, and R. Moncorgé, "CaF_2 doped with Tm^{3+}: A cluster model," J. Alloys Compd. **451**, 71-73 (2008).
4. B. Lacroix, C. Genevois, J. L. Doualan, G. Brasse, A. Braud, P. Ruterana, P. Camy, E. Talbot, R. Moncorgé, and J. Margerie, "Direct imaging of rare-earth ion clusters in Yb:CaF_2," Phys. Rev. B **90**(12), 125124-1-14 (2014).
5. C. Labbe, J.L. Doualan, P. Camy, R. Moncorgé, and M. Thuau, "The 2.8 µm laser properties of Er^{3+} doped CaF_2 crystals," Opt. Commun. **209**(1-3), 193–199 (2002).
6. F. Druon, S. Ricaud, D. N. Papadopoulos, A. Pellegrina, P. Camy, J. L. Doualan, R. Moncorgé, A. Courjaud, E. Mottay, and P. Georges, "On Yb:CaF_2 and Yb:SrF_2: review of spectroscopic and thermal properties and their impact on femtosecond and high power laser performance," Opt. Mater. Express **1**(3), 489-502 (2011).
7. G. Machinet, P. Sevillano, F. Guichard, R. Dubrasquet, P. Camy, J.L. Doualan, R. Moncorgé, P. Georges, F. Druon, D. Descamps, and E. Cormier, "High-brightness fiber laser-pumped 68 fs–2.3 W Kerr-lens mode-locked Yb: CaF_2 oscillator," Opt. Lett. **38**(20), 4008-4010 (2013).
8. E. Kaksis, G. Almási, J. A. Fülöp, A. Pugžlys, A. Baltuška, and G. Andriukaitis, "110-mJ 225-fs cryogenically cooled Yb:CaF_2 multipass amplifier," Opt. Express, **24**(25), 28915-28922 (2016).
9. W.-Z. Xue, Z.-L. Lin, H.-J. Zeng, G. Zhang, P. Loiko, L. Basyrova, A. Benayad, P. Camy, V. Petrov, X. Mateos, L. Wang, and W. Chen, "Diode-pumped mode-locked Yb:BaF_2 laser," Opt. Express **30**(9), 15807-15818 (2022).
10. P. Loiko, A. Braud, L. Guillemot, J.L. Doualan, A. Benayad, and P. Camy, "Cross-relaxation and ion clustering in Tm^{3+}:CaF_2 crystals," Proc. SPIE **11357**, 113570N (2020).
11. T. Jensen, A. Diening, G. Huber, and B. H. T. Chai, "Investigation of diode-pumped 2.8-µm Er:$LiYF_4$ lasers with various doping levels", Opt. Lett. **21**(8), 585-587 (1996).
12. M. Bernier, D. Faucher, N. Caron, and R. Vallée, "Highly stable and efficient erbium-doped 2.8 µm all fiber laser," Optics Express **17**(19), 16941-16946 (2009).
13. M. Pollnau, W. Lüthy, H. P. Weber, T. Jensen, G. Huber, A. Cassanho, H. P. Jenssen, and R. A. McFarlane, "Investigation of diode-pumped 2.8-µm laser performance in Er:BaY_2F_8," Opt. Lett. **21**(1), 48-50 (1996).
14. L. Basyrova, P. Loiko, J.-L. Doualan, A. Benayad, A. Braud, B. Viana, and P. Camy, "Thermal lensing, heat loading and power scaling of mid-infrared Er:CaF_2 lasers," Opt. Express **30**(5), 8092-8103 (2022).
15. M. Zong, Y. Wang, Z. Zhang, J. Liu, L. Zhao, J. Liu, and L. Su, "High-power 2.8 µm lasing in a lightly-doped Er: CaF_2 crystal," J. Lumin. **250**, 119089 (2022).
16. W. Ma, X. Qian, J. Wang, J. Liu, X. Fan, J. Liu, L. Su, and J. Xu, "Highly efficient dual-wavelength mid-infrared CW laser in diode end-pumped Er:SrF_2 single crystals," Sci. Rep. **6**, 36635-1-7 (2016).
17. R. Švejkar, J. Šulc, H. Jelínková, V. Kubeček, W. Ma, D. Jiang, Q. Wu, and L. Su, "Diode-pumped Er: SrF_2 laser tunable at 2.7 µm," Opt. Mater. Express **8**(4), 1025-1030 (2018).
18. J. Liu, X. Feng, X. Fan, Z. Zhang, B. Zhang, J. Liu, and L. Su, "Efficient continuous-wave and passive Q-switched mode-locked Er^{3+}:CaF_2–SrF_2 lasers in the mid-infrared region," Opt. Lett. **43**(10), 2418-2421 (2018).
19. E. E. Brown, Z. D. Fleischman, J. McKay, and M. Dubinskii, "Spectroscopic characterization of low-phonon Er-doped BaF_2 single crystal for mid-IR lasers," Opt. Mater. Express **11**(2), 575-584 (2021).
20. D. Klimm, M. Rabe, R. Bertram, R. Uecker, and L. Parthier, "Phase diagram analysis and crystal growth of solid solutions $Ca_{1-x}Sr_xF_2$," J. Cryst. Growth **310**(1), 152-155 (2008).
21. R.H. Nafziger, "High-Temperature Phase Relations in the System BaF_2-SrF_2," J. Am. Ceram. Soc. **54**(9), 467-467 (1971).
22. I. Nicoara, M. Stef, G. Buse, and A. Racu, "Growth and characterization of ErF_3 doped BaF_2 crystals," J. Cryst. Growth **547**, 125817 (2020).
23. R. Gee, D.C. O'Shea, and H.Z. Cummins, "Raman scattering and fluorescence in calcium fluoride," Solid State Commun. **4**(1), 43-46 (1966).
24. F. Aull and H. P. Jenssen, "Vibronic interactions in Nd:YAG resulting in nonreciprocity of absorption and stimulated emission cross sections," IEEE J. Quantum Electron. **18**(5), 925–930 (1982).
25. J.M. Serres, V. Jambunathan, P. Loiko, X. Mateos, H. Yu, H. Zhang, J. Liu, A. Lucianetti, T. Mocek, K. Yumashev, and U. Griebner, "Microchip laser operation of Yb-doped gallium garnets," Opt. Mater. Express, **6**(1), 46-57 (2016).